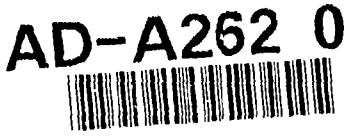

ARMY RESEARCH LABORATORY

Two-Dimensional Model for Current and Heat Transport in Solid-Armature Railguns

John D. Powell
David J. Walbert
Alexander E. Zielinski

ARL-TR-74 February 1993

NOTICES

Destroy this report when it is no longer needed. DO NOT return it to the originator.

Additional copies of this report may be obtained from the National Technical Information Service, U.S. Department of Commerce, 5285 Port Royal Road, Springfield, VA 22161.

The findings of this report are not to be construed as an official Department of the Army position, unless so designated by other authorized documents.

The use of trade names or manufacturers' names in this report does not constitute indorsement of any commercial product.

REPORT DOCUMENTATION PAGE

Form Approved
OMB No 0704-0188

1. AGENCY USE ONLY (Leave blank)	2. REPORT DATE	3. REPORT TYPE AND DATES COVERED
	February 1993	Final, Oct 91 - Sep 92

4. TITLE AND SUBTITLE

Two-Dimensional Model for Current and Heat Transport in Solid-Armature Railguns

5. FUNDING NUMBERS

PR: 1L161102AH43

6. AUTHOR(S)

John D. Powell, David J. Walbert, and Alexander E. Zielinski

7. PERFORMING ORGANIZATION NAME(S) AND ADDRESS(ES)

U.S. Army Research Laboratory
ATTN: AMSRL-WT-WD
Aberdeen Proving Ground, MD 21005-5066

8. PERFORMING ORGANIZATION REPORT NUMBER

9. SPONSORING/MONITORING AGENCY NAME(S) AND ADDRESS(ES)

U.S. Army Research Laboratory
ATTN: AMSRL-OP-CI-B (Tech Lib)
Aberdeen Proving Ground, MD 21005-5066

10. SPONSORING/MONITORING AGENCY REPORT NUMBER

ARL-TR-74

11. SUPPLEMENTARY NOTES

12a. DISTRIBUTION/AVAILABILITY STATEMENT

Approved for public release; distribution is unlimited.

12b. DISTRIBUTION CODE

13. ABSTRACT (Maximum 200 words)

A numerical model is developed for solving the equations which predict current and heat transport in a solid-armature railgun. The model is two dimensional and fully time dependent. Some preliminary calculations are carried out for a "U-shaped" armature similar to that currently under investigation in the ARDEC small- and cannon-caliber railgun programs. The most extensive calculations are for a situation in which the projectile is started at rest and accelerated to about 500 m/s in a time of about 1 ms. Results of the calculations can be used to infer, for example, where melting in the armature is most likely to occur and where the electromagnetic stresses are largest. For comparison, calculations are also presented for a situation in which the projectile is held fixed. Some discussion of future efforts is given, with particular emphasis on describing how the model might be used to guide the design of armatures, or provide input for other types of calculations relating to electromagnetic guns.

14. SUBJECT TERMS

electromagnetism; railgun; electrodynamics; electromagnetic propulsion; electromagnetic launch; electromagnetic guns

15. NUMBER OF PAGES

31

16. PRICE CODE

17. SECURITY CLASSIFICATION OF REPORT	18. SECURITY CLASSIFICATION OF THIS PAGE	19. SECURITY CLASSIFICATION OF ABSTRACT	20. LIMITATION OF ABSTRACT
UNCLASSIFIED	UNCLASSIFIED	UNCLASSIFIED	UL

INTENTIONALLY LEFT BLANK.

TABLE OF CONTENTS

INTENTIONALLY LEFT BLANK.

LIST OF FIGURES

LIST OF TABLES

INTENTIONALLY LEFT BLANK.

Acknowledgment

We thank Mr. Larry Burton and Dr. Steven Cornelison for their careful reviews of this manuscript.

INTENTIONALLY LEFT BLANK.

1. INTRODUCTION

In recent years, much effort has been expended in the research and development of various types of armatures to be used with electromagnetic railguns. Each of these types of armatures is believed to have a unique set of applications, and it is important to assess conditions under which they will perform in a satisfactory manner. In this report we will be concerned with studying the time-dependent diffusion of current and the resultant heating, both in the rails and in the armature, in a solid-armature railgun. An understanding of this problem is important in order to guide the design of projectiles, in order to determine the limits under which these armatures can operate, and in order to study the dynamics of the armature and the gun tube.

A schematic diagram of a simple railgun, indicating the general principles on which it operates, is shown in Fig. 1. Current supplied by the power supply flows down one rail, through the armature, and back along the other rail. The interaction of the current through the armature with the magnetic field produces a Lorentz force which accelerates the armature and projectile down the rails. The subject of concern here is the distribution of current, the resulting body forces, and the generation and transport of heat in both the rails and armature.

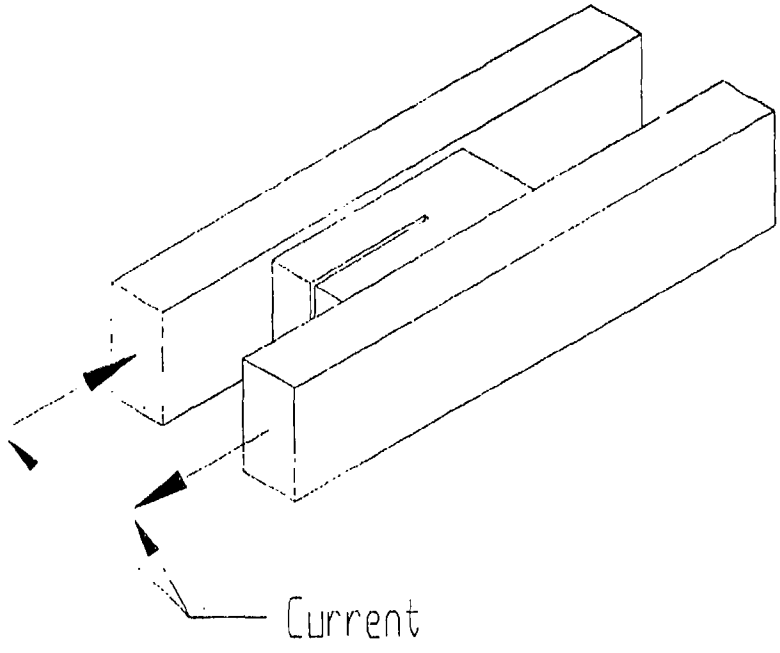

Figure 1. Schematic Diagram of Solid-Armature Railgun.

Similar types of calculations have been undertaken by various investigators in the past. In early work, Hughes and Young (1982) investigated analytically the current-diffusion prob-

lem in the steady state for some rather simple types of armature geometry. Their work provided considerable insight into how the current could be expected to vary and the practical problems that would be encountered as the projectile velocity increased. Later their work was extended to a transient analysis and some limiting-case, exact solutions were obtained (1986). Similar transient, exact calculations have been undertaken by Nearing and Huerta (1989). Probably the most thoroughgoing treatment of the problem is the work performed by Long (1986) a few years ago. His early analysis was steady state, somewhat similar to that of Hughes and Young, and succeeded in predicting the current distribution analytically for simple rectangular projectiles and rather low armature velocities. In later graduate-thesis work, Long (1987) developed a finite-element program with which he successfully studied more complicated armatures at higher velocities. In addition, he included the effects of Joule heating and heat transport, which had been neglected in the earlier analytic calculations. In more recent work, Putley (1989) adapted a previously developed code to solve the rail-armature interaction problem, verified some of Long's earlier calculations that were done analytically, and extended calculations to somewhat higher velocities. All of these calculations have been two dimensional so that the rails were assumed to be infinitely high, with no variation in physical quantities along the direction of the rail height allowed.

Still more recent are the important efforts underway to perform diffusion calculations in moving conductors in three dimensions. This work has been described in several references (Rodger, Leonard, Eastman, and Atkinson 1989; Rodger, Leonard, and Eastman 1991; Rodger and Leonard 1991). The three-dimensional calculations should ultimately provide a realistic indication of the current and temperature distributions in railguns, since these models can be used to avoid many assumptions of very limited applicability associated with the infinite rail-height calculations. However, the work is considerably more complicated than in two dimensions and is rather preliminary at this point.

The calculations to be undertaken here are most similar to those carried out by Long. We have developed a two-dimensional, finite-difference program which solves the governing equations for the fully transient case. Our motivation has been to provide information which could be used in the design of projectiles, as well as possibly to provide information which could eventually be used as input in stress-analysis codes which have been developed to investigate gun-tube dynamics. The calculations here represent our first effort in the application of this code, and we restrict ourselves to investigating diffusion in the "U-shaped" armature currently under study in the ARDEC, small- and cannon-caliber, electromagnetic-gun programs. While such armatures have some disadvantages in real use, this type of geometry (trailing chevron) represents a large body of research in the electromagnetic-gun community and has been found to be reasonably successful for launch at high velocities

(Barber and Challita 1992).

The organization of the report is as follows. In Sec. 2, the model is described and the mathematical formalism developed. In Sec. 3, we describe the results of some calculations for a specific armature geometry. Finally, Sec. 4 contains our discussion, summary, and conclusions.

2. MODEL AND FORMALISM

2.1 Governing Equations. The basic equations that must be solved numerically consist of the appropriate Maxwell equations as well as the energy transport equation for the rails and projectile. It is convenient to solve these equations in a frame of reference in which the armature is fixed with its trailing edge located at $x = 0$, and the rails move in the negative x direction. We will restrict ourselves to situations in which the armature is symmetric about a plane normal to and centered between the two rails. This plane is defined by $y = 0$ (see Fig. 2). The rails and projectile are infinitely extended in the z direction.

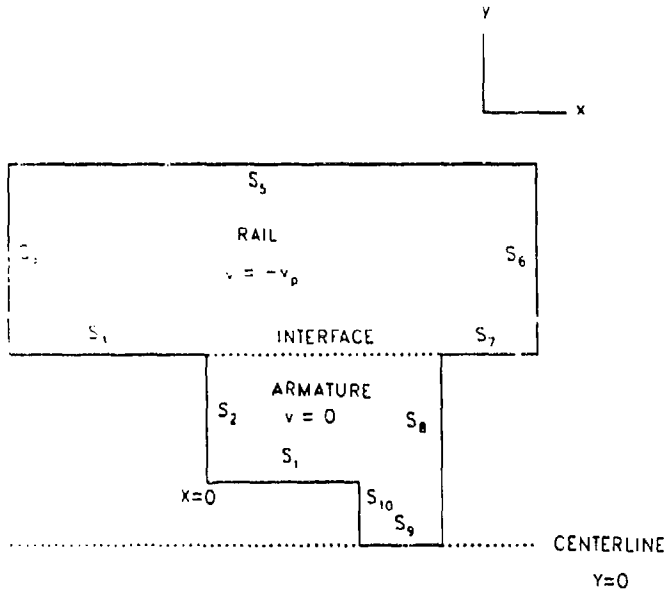

Figure 2. Schematic Diagram of Rail-Armature Model.

Let $\vec{J}$, $\vec{B}$, and $\vec{E}$ be the current density, the magnetic induction field, and the electric field intensity. Let μ, κ, σ, and C be the magnetic permeability, the thermal conductivity, the electrical conductivity, and the specific heat. Finally, let T, ρ, and v be the temperature, density, and material velocity at a given point in the rail-armature system. The governing

Maxwell equations can then be written

$$\nabla \times \vec{B} = \mu \vec{J}, \tag{1}$$

$$\nabla \times \vec{E} = -\frac{\partial \vec{B}}{\partial t}, \tag{2}$$

and

$$\vec{J} = \sigma(\vec{E} + \vec{v} \times \vec{B}). \tag{3}$$

As is customary in calculations of this type, we have neglected the displacement current in Eq. (1). This approximation can be shown to be valid provided the armature velocity is small compared to the light speed c, and provided the time scale τ of the problem satisfies the condition $\tau >> (\mu\sigma c^2)^{-1}$. Both these conditions are very easily satisfied for rail-launcher problems.

We now observe that for the infinite rail-height geometry discussed above, we must have that $\vec{B} = B\hat{a}_z$ and that J_z and E_z both vanish. Furthermore, there can be no z dependence in any of the physical quantities. If we now make use of these observations we find that Eqs. (1)-(3) can be uncoupled to produce a single, second-order, partial differential equation which predicts the convection and diffusion of the magnetic induction field. The equation can be written

$$\mu\sigma\frac{\partial B}{\partial t} = \frac{\partial^2 B}{\partial x^2} + \frac{\partial^2 B}{\partial y^2} - \mu\sigma v\frac{\partial B}{\partial x} - \frac{1}{\sigma}\frac{\partial \sigma}{\partial T}\frac{\partial T}{\partial x}\frac{\partial B}{\partial x} - \frac{1}{\sigma}\frac{\partial \sigma}{\partial T}\frac{\partial T}{\partial y}\frac{\partial B}{\partial y}. \tag{4}$$

In obtaining Eq. (4), we have assumed that σ depends on position and time only through the temperature T.

A similar assumption for κ and C allows us to write the heat-transport equation as

$$\rho C\frac{\partial T}{\partial t} + \rho v C\frac{\partial T}{\partial x} = \frac{1}{\mu^2\sigma}\left[\left(\frac{\partial B}{\partial x}\right)^2 + \left(\frac{\partial B}{\partial y}\right)^2\right] + \frac{\partial \kappa}{\partial T}\left(\frac{\partial T}{\partial x}\right)^2 + \frac{\partial \kappa}{\partial T}\left(\frac{\partial T}{\partial y}\right)^2 + \kappa\frac{\partial^2 T}{\partial x^2} + \kappa\frac{\partial^2 T}{\partial y^2}. \tag{5}$$

The meaning of the various terms which appear in Eq. (5) are rather obvious except perhaps for the term enclosed in brackets on the right-hand side. If, however, we use Eq. (3) we can identify this term as being equal to J^2/σ, and thus accounting for resistive heating in the armature and rails.

Equations (4) and (5) are the basic differential equations which must be solved subject to some set of initial and boundary conditions. It is evident upon examination of the equations that, provided the initial conditions satisfy the conditions $B(y) = B(-y)$ and $T(y) = T(-y)$, symmetry about $y = 0$ will persist for all time. We will restrict ourselves to this case and only solve the equations for $y \geq 0$.

2.2 Boundary Conditions. A schematic diagram of the rail-armature configuration for $y \geq 0$ is shown in Fig. 2. The armature is assumed to be the trailing-chevron type discussed previously, but the analysis can be easily extended to other types of geometry. We assume that there is no heat transfer between conductors and their surroundings so that at all conductor surfaces we have

$$\hat{n} \cdot \nabla T = 0 \tag{6}$$

where $\hat{n}$ is the unit normal to the surface (pointing into the conductor). Such a condition also applies along the centerline S_9 from symmetry.

For a given total current input, boundary conditions on the magnetic induction field can be easily determined along most surfaces from Ampere's law. If we let j be the current per unit rail height then we must have

$$B = \mu j \qquad along\ S_1, S_2, S_3, and\ S_{10} \tag{7}$$

and

$$B = 0 \qquad along\ S_5, S_6, S_7, and\ S_8. \tag{8}$$

From symmetry we have

$$\frac{\partial B}{\partial y} = 0 \qquad along\ S_9, \tag{9}$$

and along the rail end we assume that current enters and leaves parallel to the x axis so

$$\frac{\partial B}{\partial x} = 0 \qquad along\ S_4. \tag{10}$$

In order for the last assumption to be valid, the breech end of the rails should be sufficiently far away from the projectile that the current distribution at the breech is not affected by the projectile motion. An alternative approach, which we will investigate in the future, is to solve Eq. (4) in the rails via a shooting technique in which we proceed along the negative x direction until we reach the point at which $\frac{\partial B}{\partial x} \simeq 0$.

In general we will take the rails and armature to be different materials. As a result, $\partial T/\partial y$ and $\partial B/\partial y$ are not continuous across the rail-armature interface. The appropriate jump conditions that apply at the boundary can be obtained by integrating Eqs. (4) and (5) across the interface, assumed to have thickness ϵ, and then taking the limit as $\epsilon \to 0$. We find

$$\left[\frac{1}{\sigma}\frac{\partial B}{\partial y}\right] = 0 \qquad at\ the\ interface, \tag{11}$$

and

$$\left[\kappa\frac{\partial T}{\partial y}\right] = 0 \qquad at\ the\ interface, \tag{12}$$

where the brackets (here only) denote the change in the quantity enclosed as the interface is crossed.

2.3 <u>Numerical Procedure</u>. To solve Eqs. (4) and (5), we developed both explicit and, later, implicit finite-difference codes. The grid spacing was taken to be nonuniform. In the explicit calculations, the solution at interior grid points was marched forward in time beginning with some prescribed set of initial conditions at time $t = 0$. Once the interior solutions were obtained, conditions at the boundaries were extrapolated, via formulas in the preceding section, for situations in which the surface conditions were the Neumann type. A similar procedure was used to obtain values of B and T at the interface such that they were in compliance with Eqs. (11) and (12). At all corners we generally required that $\partial T/\partial x$=0, but also undertook some calculations in which the boundary condition was $\partial T/\partial y$=0. Little difference in the results was observed except very near corners whose interior angle (measured in the conductor) exceeded 180 degrees. This point is subsequently discussed in greater detail.

Reasonable values for both the time step and the grid spacing were determined largely by trial and error, and these parameters were varied in a number of calculations to demonstrate consistency of the solution. Quite generally, we chose a grid spacing that satisfied the condition (Putley 1989)

$$\mu\sigma|v|\Delta < 1, \tag{13}$$

at least in regions where we expected there to be a significant current density. The variable Δ is taken to imply Δx or Δy. The quantity on the left-hand side of Eq. (13) can be recognized as the magnetic Reynolds number, with the characteristic length given by the grid spacing.

In our initial calculations with the explicit code, we employed a central-difference, forward-time approximation, but encountered some numerical stability problems at velocities greater than about 100 m/s. We found that these problems could be considerably ameliorated by using first-order, upwind differencing for the convective terms in the rails where the velocity was not equal to zero. To get some idea of the size of the time step necessary to insure stability, we analyzed the numerical stability characteristics of the simple convection-diffusion equation

$$\alpha\frac{\partial F}{\partial t} = \frac{\partial^2 F}{\partial x^2} - \alpha v\frac{\partial F}{\partial x}, \tag{14}$$

where α is constant. That Eq. (14) is a linearized, one-dimensional, limiting-case version of Eqs. (4) and (5) is evident. The stability analysis was undertaken under the assumption that the grid spacing was constant and that the first-order spatial derivatives could be approximated by a first-order, upwind differencing approximation; second derivatives were approximated by central differences. The analysis led to a condition on the time step necessary to insure stability, namely,

$$\Delta t \leq \frac{2\alpha\Delta x^2 + |v|\alpha^2\Delta x^3}{4 + v^2\alpha^2\Delta x^2 + 4|v|\alpha\Delta x}. \tag{15}$$

For small velocities where convection is negligible one obtains the usual diffusion-equation result that $\Delta t \leq \alpha\Delta x^2/2$; for large velocities one finds the Courant condition $\Delta t \leq \Delta x/|v|$. For values of α relevant to the problem under study here, the criterion in Eq. (15) is found to be less restrictive than that obtained when central differencing is used in the convective terms.

The code was rewritten with an implicit formulation of the difference equations when we found the time step required in the explicit version to be excessively small, particularly

at high projectile velocities. In the implicit calculations, the coupled algebraic equations resulting from the finite-difference approximations were solved by an iterative overrelaxation procedure (Ames 1977). Restrictions on the grid spacing were kept the same as in the explicit case, but we found much longer time steps acceptable.

The calculations discussed in this report were undertaken with both the explicit and implicit codes, and we produced the same results to within a very high degree of accuracy. In the explicit calculations, it was necessary to take time steps of 5-10 ns; in the implicit version, on the other hand, time steps of 0.5-2 μs proved satisfactory and the greater magnitude of the time step led to a considerable reduction in computer time.

3. CALCULATIONS

We now discuss some calculations which were undertaken with the numerical model for the trailing-chevron armature previously discussed. The rails were taken to be 1 cm thick and separated by a distance w equal to 1.5 cm. The armature was 3.55 cm long and contained a slot, 23 mm long and 1 mm wide, located in the center of the armature at the trailing edge. This particular configuration for both the rails and the armature was chosen to be consistent with experiments which we plan to do in the near future. The geometry is shown for $y \geq 0$ in Fig. 3. Also shown in that figure is a schematic of the grid used in the calculation. The minimum grid spacing is at the left-hand end of the armature-rail interface ($x = 0, y = 7.5\ mm$) with values of Δx and Δy of about $5 \times 10^{-5}\ m$. Of course, the rails in general extend farther, in both the positive and negative directions, than is shown in the figure. In the calculations, we accounted for all the rail to the left of the armature, but neglected that to the right at distances greater than $x = 50\ mm$. The justification for neglecting this forward portion of the rails is that both the fields and the temperature decay very rapidly ahead of the armature.

It is necessary to supply as input into the calculation the total current per unit rail height as a function of time. We have used a profile obtained from a lumped-parameter analysis for the BRL 400 kJ, capacitive power supply (Powell and Zielinski 1992), driving the 1.5 cm, square-bore railgun which we propose to use in future experiments. The functional form is given by

$$\begin{aligned} j &= j_0\, sin(\frac{\pi t}{t_0}) && for\ t \leq t_0 \\ j &= j_0\, exp[-(t - t_0)/t_1] && for\ t \geq t_0 \end{aligned} \tag{16}$$

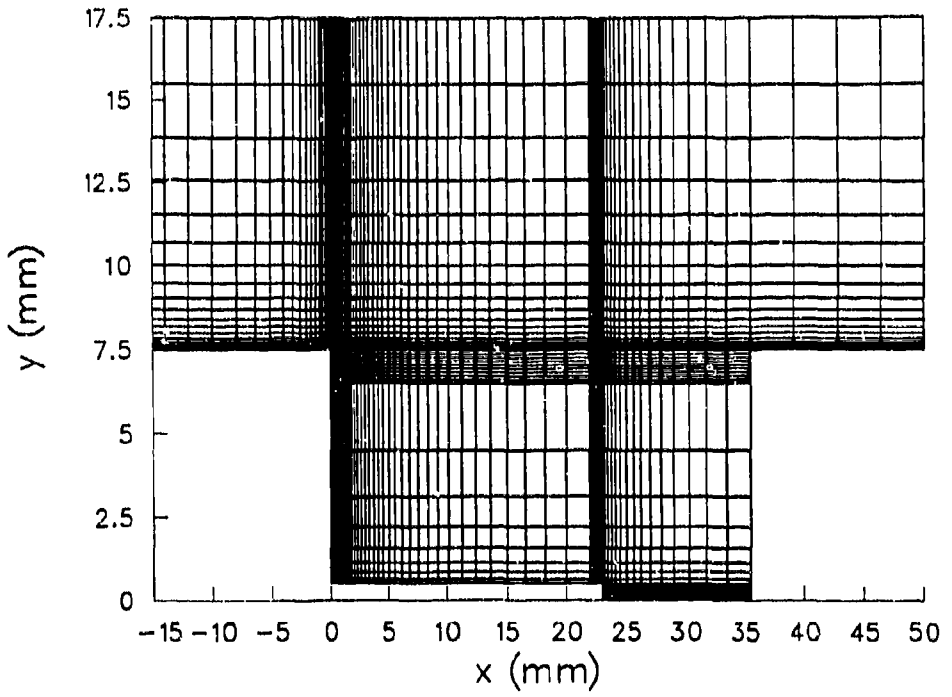

Figure 3. Geometry and Grid for Calculations.

where $j_0 = 17.8\ MA/m$, $t_0 = 260\ \mu s$, and $t_1 = 2029\ \mu s$. In principle, no additional information need be provided in order to carry out the calculation, since the projectile velocity v_P can be computed from the appropriate electromagnetic forces. However, it is well known that two-dimensional, infinite rail-height models significantly overestimate the magnitude of that velocity. To obtain a more realistic estimate, we have assumed that the armature acceleration was proportional to j^2 at any time, calculated the resulting functional form for the velocity, and then determined the integration constant from an estimated value of v_P at time $t = t_0$. This estimate of the velocity via calculation from the measured inductance gradient of the railgun and the assumed armature mass of 18.7 g. We then find that the projectile velocity satisfies the equation

$$v_P = \frac{v_0}{t_0}\left[t - \frac{sin(\pi t/2t_0)}{(\pi/t_0)}\right] \qquad t \leq t_0$$

$$v_P = v_0 + \frac{v_0 t_1}{t_0}\left[1 - e^{-2(t-t_0)/t_1}\right] \qquad t \geq t_0. \tag{17}$$

The material velocity in the rails, of course, is given by $v = -v_P$, while that in the armature is zero. The numerical value of v_0 was 101 m/s. For asymptotically large values of the time, we have $v_P = v_0(1 + t_1/t_0) \simeq 890\ m/s$.

The armature displacement S can be determined by further integration of Eq. (17) and

we find

$$S = \frac{v_0 t^2}{2t_0} + \frac{v_0 t_0}{\pi^2}[cos(\pi t/t_0) - 1] \qquad t \le t_0$$

$$S = v_0 t_0(1/2 - 2/\pi^2) + v_0(t - t_0)(1 + t_1/t_0) + \frac{v_0 t_1^2}{2t_0}\{exp[-2(t - t_0)/t_1] - 1\} \qquad t \ge t_0. \quad (18)$$

Graphs of j, v_P, and S are shown in Fig. 4 for the first 2 ms of the simulation. Each quantity is normalized by its maximum value in the time interval, i.e., by 17.8 MA/m, by 747 m/s, and by 0.90 m, respectively.

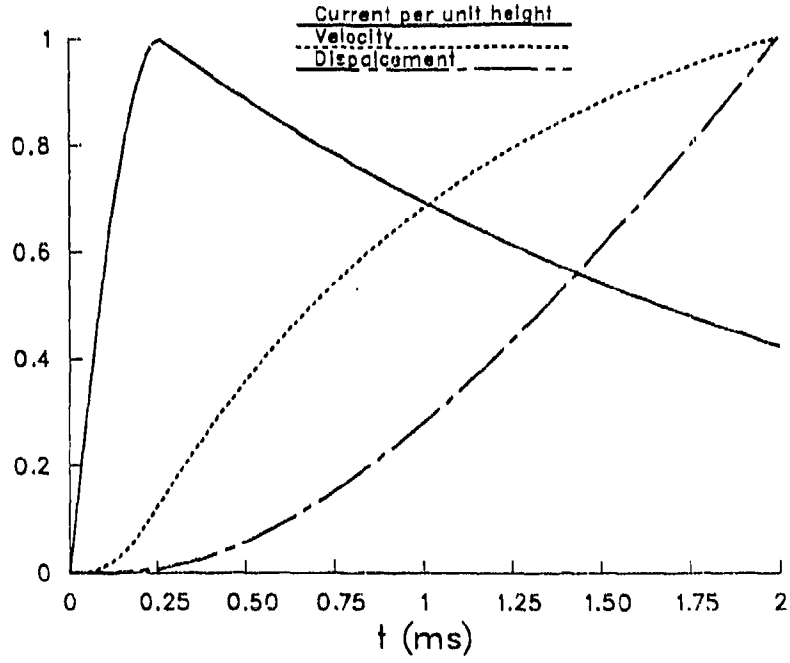

Figure 4. Current per Unit Rail Height, Projectile Velocity, and Projectile Displacement as a Function of Time. Quantities are normalized by the values given in the text.

We performed the calculations under the assumption that the rails were copper and the armature was aluminum. Material properties were provided by approximate curve fits which we computed as a function of temperature. These properties are appropriate for the solid phase and we did not account for any change of phase in either the rails or the armature when the temperature at some point became sufficiently high. Consequently, our interest was in determining where high temperatures were most likely to occur, and not in describing the behavior of the material outside the solid regime. The data used in the calculations are shown in Table 1.

For all calculations we took the initial value of the magnetic induction to be zero and

Table 1. Material Properties for Copper and Aluminum Used in Calculation

	Copper	Aluminum
σ	$4.41 \times 10^7/[1 + 0.0039(T - 300)]$ mho/m	$3.21 \times 10^7/[1 + 0.0039(T - 300)]$ mho/m
C	$0.0987T + 355$ $J/(K\ kg)$	$0.486T + 766$ $J/(K\ kg)$
ρ	8900 kg/m^3	2700 kg/m^3
κ	400 $W/(m\ K)$	205 $W/(m\ K)$

the temperature in the conductors to be 300 K. For the calculations described here, the initial position of the left-hand end of the rail was approximately 2 cm from the left surface of the projectile located at $x = 0$. We have, however, also done calculations in which that initial distance was taken to 16 cm. These calculations were performed in order to test the validity of the assumption made in [10]. Both calculations produced similar results in the armature and in the rails at points close to the rail-armature interface.

At time $t = 0$, we applied the boundary conditions discussed previously and solved Eqs. (4) and (5) via the procedure discussed in the previous section. Two different calculations were performed: In the first, the projectile velocity varied according to the relation in Eq. (17); in the second, the projectile was held fixed with $v_P = 0$.

We will present results of the calculations as a series of graphs which show at various times during the course of the calculation (1) lines of constant induction (current streamlines) within the rails and armature; (2) the force normal to the armature perimeter; (3) the temperature along the armature perimeter; (4) the temperature along the in-bore surface of the rail; and (5) lines of constant temperature (isotherms) within the armature.

Shown in Figs. (5)-(7) are lines of constant magnetic induction in both the armature and projectile. These lines are plotted at 200 μs intervals until the calculation was terminated at 1 ms. The x coordinate in the graphs was transformed so as to reflect the actual motion of the projectile. More specifically, we have plotted these results as a function of the coordinate $X{=}x - x_{end}$ where x_{end} denotes the location of the left-hand end of the rail in the frame of reference in which the projectile is fixed.

At time $t = 0$, shown in Fig. 5, the field is everywhere zero since the total current is initially zero. As the current begins to rise, the field begins to diffuse away from surfaces S_1, S_2, S_3, and S_{10}, where the boundary condition is nonzero. By 200 μs, a significant amount of diffusion has occurred. The curve nearest to the surfaces above represents the locus of points where the magnetic induction is 75% of its value at the surface; the second and third curves indicate points where the field is 50 and 25%, respectively. The field diffuses somewhat

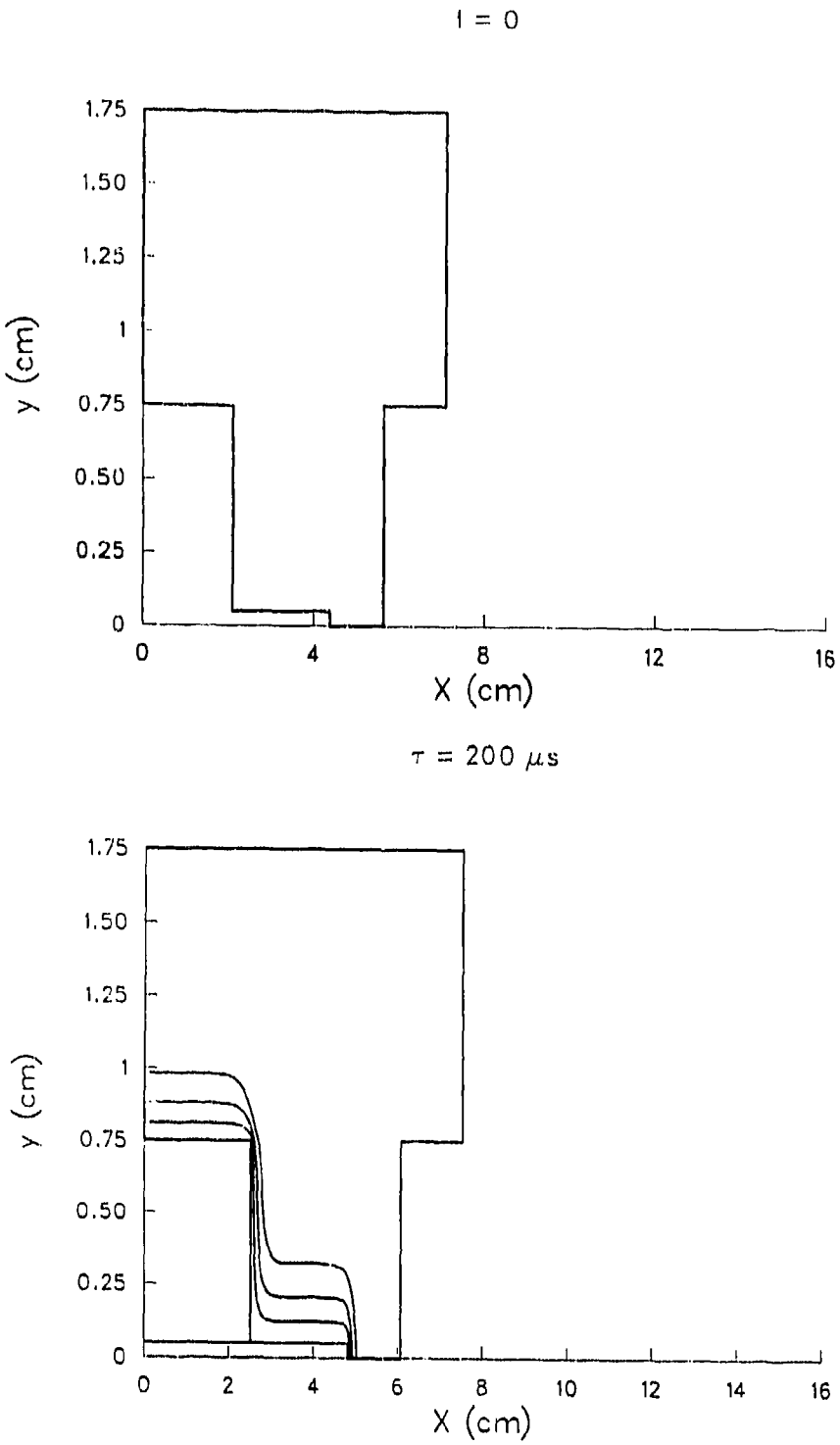

Figure 5. Lines of Constant Magnetic Induction at $t = 0$ and $t = 200\ \mu s$.

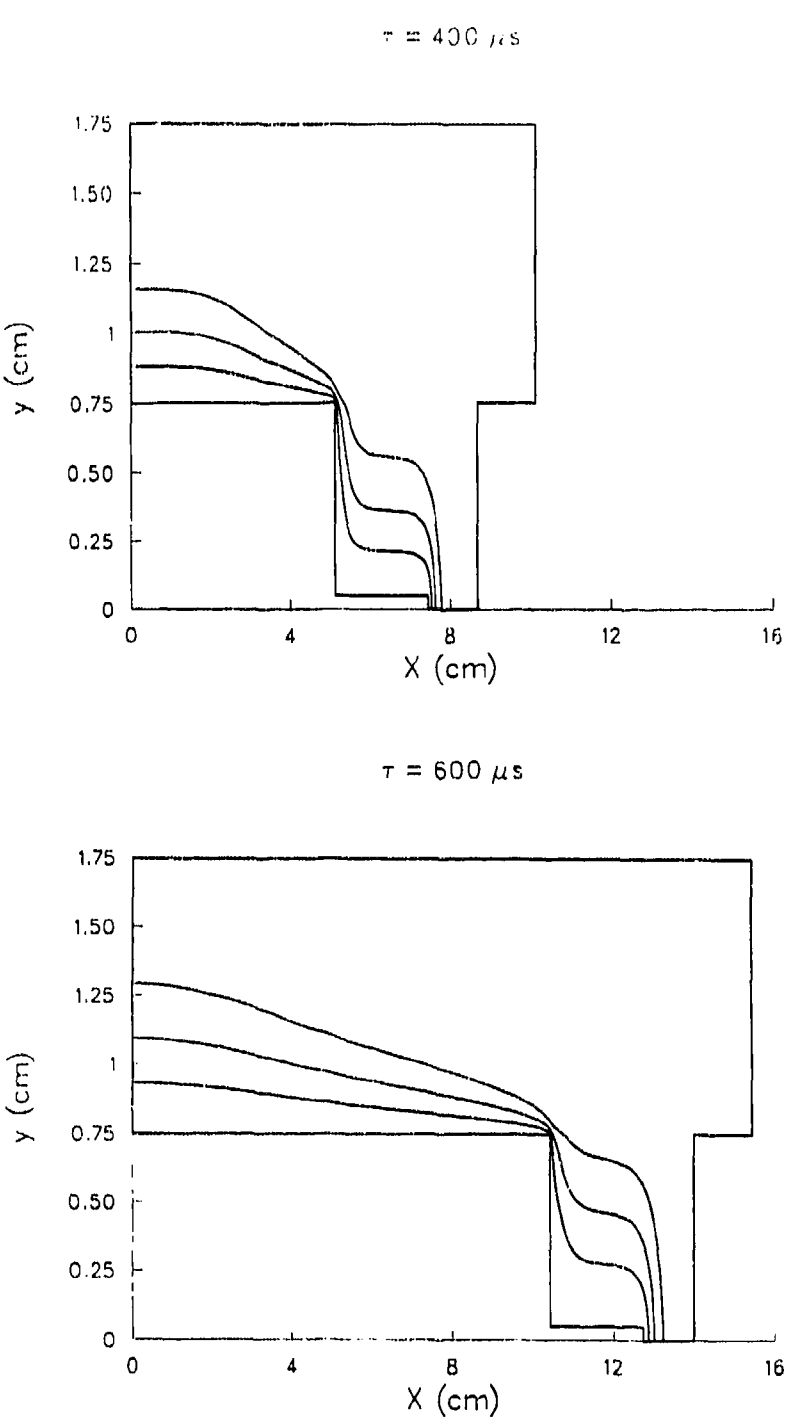

Figure 6. Lines of Constant Magnetic Induction at 400 and 600 μs.

τ = 800 μs

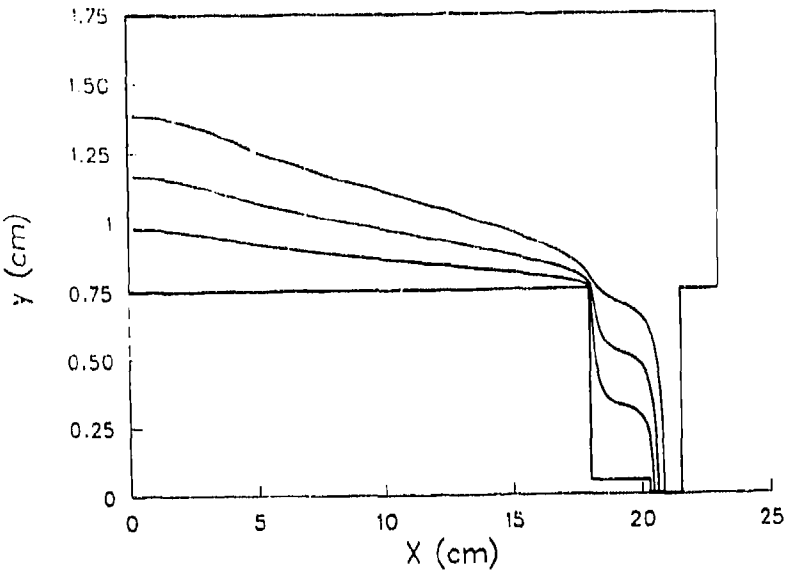

τ = 1000 μs

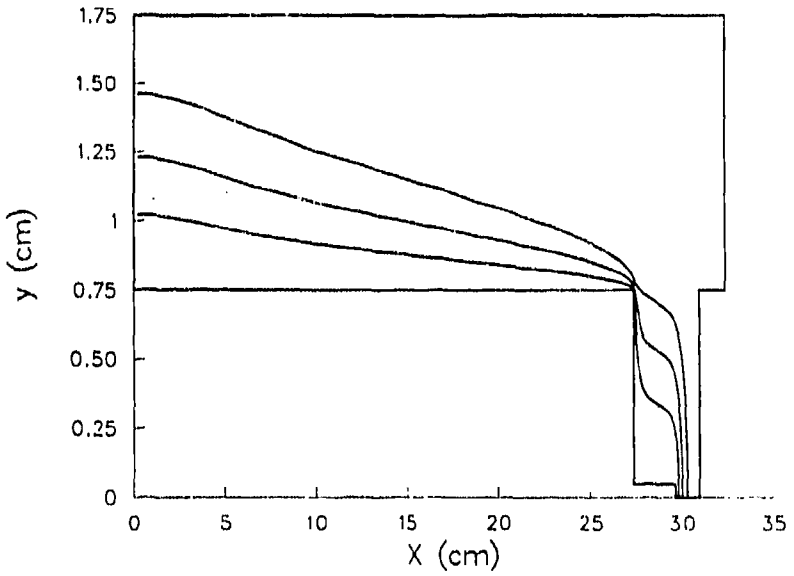

Figure 7. Lines of Constant Magnetic Induction at 800 and 1000 μs.

more rapidly in the aluminum than in the copper because of the lower conductivity.

The physical significance of the lines of constant induction is that they also represent current streamlines. In particular, it is possible to prove from Maxwell's equations that the current can never cross lines of constant induction, so that these lines represent the general path taken by the current. Consequently, 25% of the total current is contained between successive lines in Figs. (5)-(7).

At later times, shown in Figs. 6 and 7, additional diffusion is evident, as is substantial displacement of the projectile. At 1 ms, the projectile has travelled about 25 cm and its velocity is about 500 m/s. Virtually complete diffusion has occurred throughout both the rails and projectile by this time. The most noteworthy aspect of the results is the high concentration of current in the left-hand end of the rail-armature interface. This concentration, which increases with increasing velocity, is referred to as the velocity skin effect and will be discussed in more detail in the following section.

We have also plotted, at the same time intervals, the temperature along the perimeter of the armature and along the in-bore rail surface. Distance along the armature perimeter, s, is defined such that $s = 0$ corresponds to the left-hand side of the rail-armature interface, and s increases as one moves counterclockwise around the armature surface. For the problem at hand, the maximum value of s is 3.05 cm and this point is located at the slot corner between side S_9 and S_{10}. Other values of s along the armature perimeter are shown in Fig. 8.

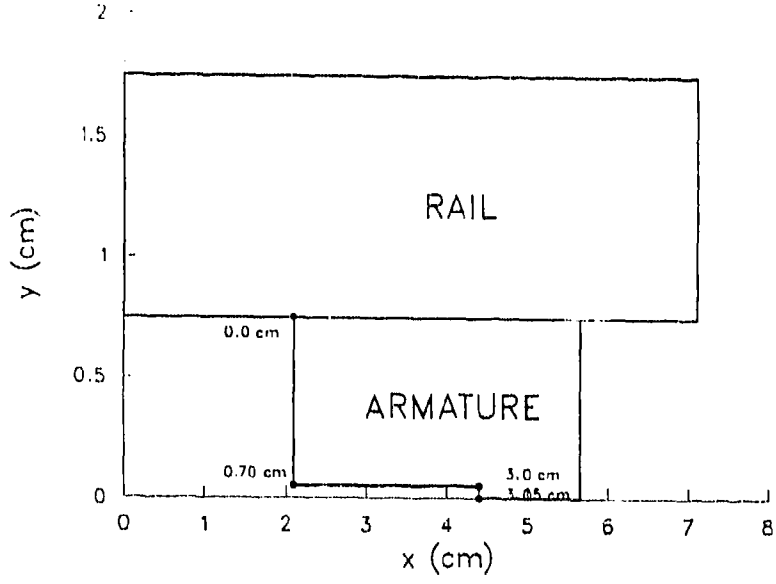

Figure 8. Definition of Distance s Around the Armature Perimeter.

The temperature as a function of s is shown in Fig. 9. It should be noted that, except near the corners, there is not significant change in the temperature as time progresses. This behavior apparently results because heat generated resistively near the conductor surface is almost completely conducted into the interior of the solid. It is known, for example, that when a magnetic field is established at the surface of a conductor, there is an initial rise in the surface temperature by an amount proportional to B^2. Subsequently, however, the temperature does not change significantly until such time as the current has completely diffused and bulk heating has become important. This phenomenon is sometimes referred to as the "one-third B^2 law," since the constant of proportionality indicated above is about one third for most conductors if B is measured in Tesla and T in degrees Kelvin. The effect has been discussed in some detail by Barber (1972).

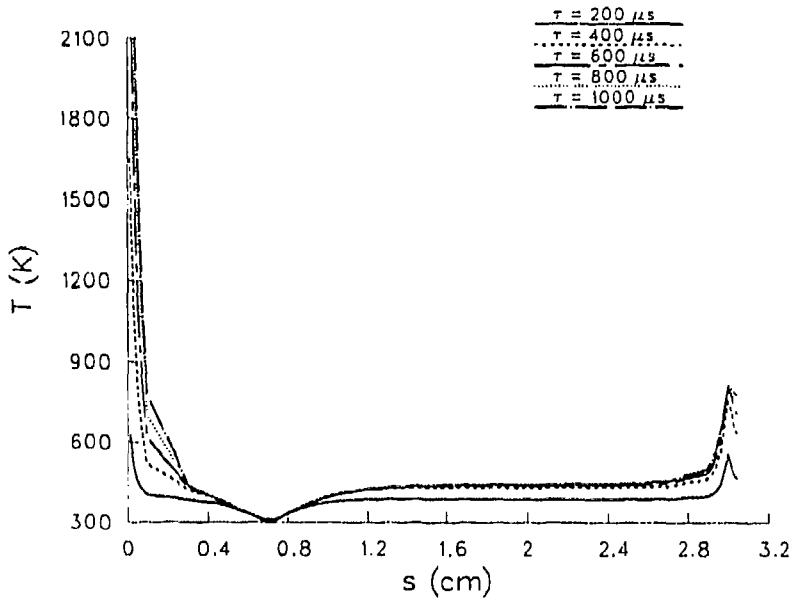

Figure 9. Temperature as a Function of Distance s Along the Armature Perimeter.

There is quite a significant rise in temperature at the corner of the rail-armature interface and, to a lesser extent, at the corner of the slot between sides S_1 and S_{10}. These high temperatures obviously result from the high current concentrations in those corners as was seen in Figs. 4-6. Similarly, there is virtually no heating at the corner between sides S_1 and S_2 because of the small concentration of current there. We can, in fact, make the rather crude generalization that corners for which the angle between sides (measured in the conductor) is greater than 180 degrees tend to be hot, whereas those for which the angle is less than 180 degrees are relatively cool.

It may also be observed that the gradients in the temperature become very large near

the large-angle corners. In fact, it has been shown that these gradients are infinite for the solution of Laplace-type equations at the location of the corner (Ames 1977). The problem undoubtedly introduces some numerical error in the solutions obtained here especially in the vicinity of the corner. Additional discussion of this problem and efforts we have made to analyze the extent of the error are discussed in the next section.

In Fig. 10 is shown the temperature along the in-bore rail surface (i. e., along the line $y = 7.5\ mm$) beginning at the trailing edge of the rail ($X = 0$) and proceeding forward to the point at which the temperature just approaches the ambient value. In each of the figures plotted, the location of the corner of the rail-armature interface is evident from the extremely rapid change in temperature at the point in question. This variation near the corner is similar to that observed at the slot corner in Fig. 9. Here, however, except at very early times, the temperature to the left of the spike is higher than that observed to the left of the slot corner; these higher temperatures result from the motion of the projectile or, alternatively, convection of heated rail material in the negative x direction in the frame of reference in which the calculation was performed. Similarly, the motion of the projectile accounts for the increased steepness of the gradients near this point. It may be observed that the maximum temperature in the rails to the left of the interface occurs at a distance of about 4 cm and at a time of 600 μs. This temperature is about 410 K. At longer times the higher velocities produce some cooling owing to the more significant convection.

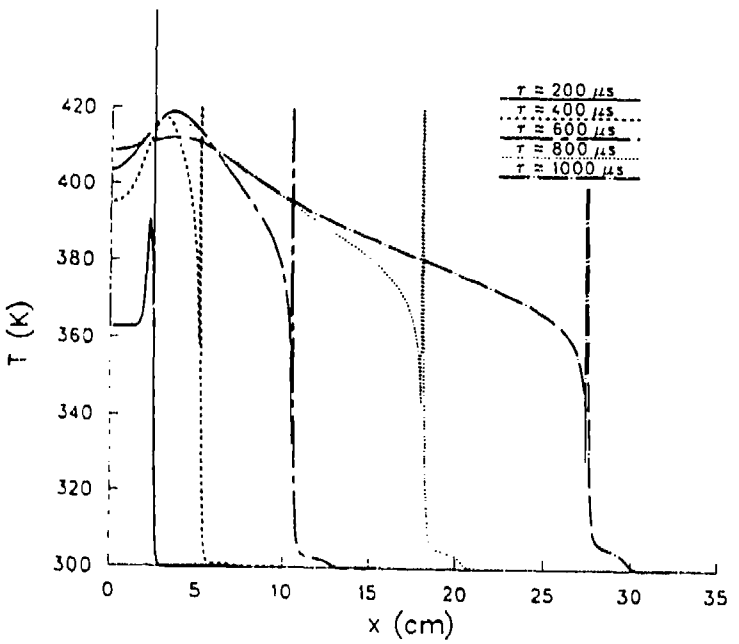

Figure 10. Temperature Along the In-Bore Rail Surface.

In Fig. 11, we show the force per unit volume F normal to the surface at points along

the armature perimeter. This force is calculated from the relation

$$F = \vec{J} \times \vec{B} \cdot \hat{n}. \tag{19}$$

The results are somewhat self-evident except for the slightly negative values near the intersection of sides S_1 and S_2. These negative forces occur only after maximum current and result from an eddy current that is produced by the decreasing induction field. This eddy current is superimposed on the main current and, at most points along the surface, is not noticeable. Because of the low concentration of the main current in this corner, however, the eddy current is actually larger in magnitude. The motivation for computing these forces at various points in the armature is that they may be used to help evaluate rail-armature contact performance. We should point out, however, that a two-dimensional model will substantially overestimate these internal forces for the same reasons that such a model overestimates the velocity imparted to the projectile.

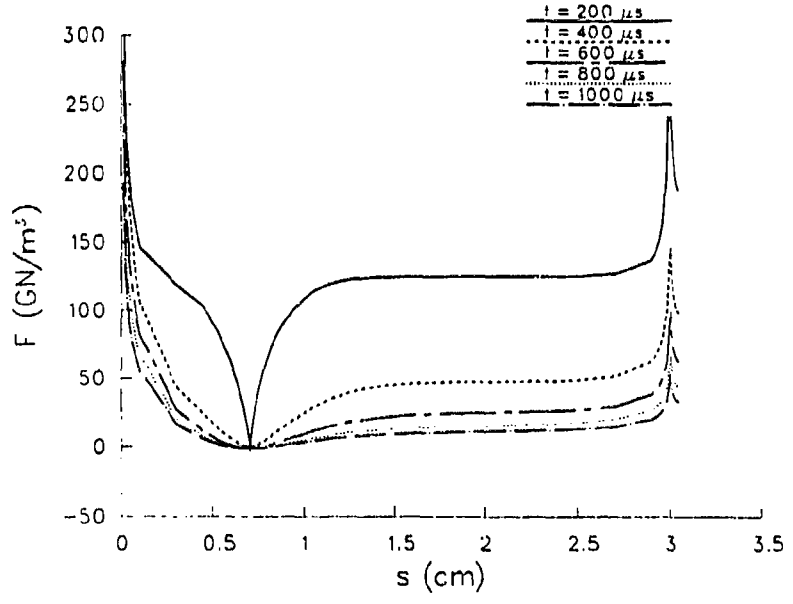

Figure 11. Normal Force as a Function of Distance s Along the Armature Perimeter.

Finally, we show in Fig. 12 isotherms within the armature at $t = 800\ \mu s$. As has been pointed out before, the temperature is highest near large-angle corners and lowest near small-angle corners. Of course, the temperature approaches ambient at distances far removed from those surfaces where the B field is zero.

We have also carried out, for purposes of comparison, a number of calculations in which the projectile velocity was held fixed at zero. These calculations were carried out for some-

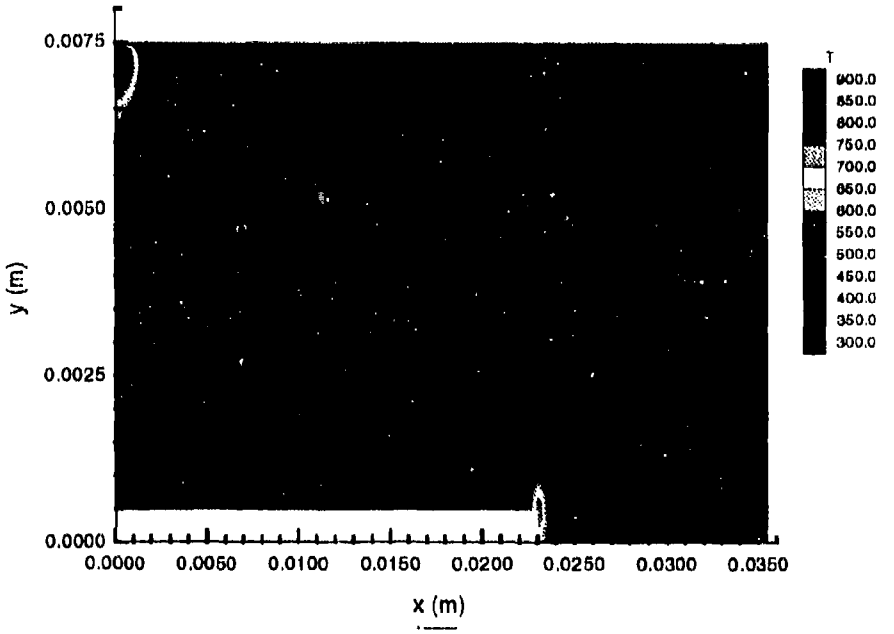

Figure 12. Isotherms Within the Armature at 800 μs.

what larger times, namely, to about 1600 μs. The more extensive calculations can be done fairly easily for this case because numerical problems caused by large projectile velocities are not present. We will describe only some of the more significant results.

Results for the current streamlines at 800 μs are shown in Fig. 13. As is quite evident from the figure, there is not the high concentration of current in the corner of the rail-armature interface that was present in the previous case. The extent of concentration, which increases with increasing velocity, is referred to as the velocity skin effect and can be described physically as follows. At low projectile velocities, there exists sufficient time for current to diffuse into the rails during the time that the projectile is in contact with a given point on the rail surface. Consequently, the resistance along the interface can decrease significantly during the time of contact. On the other hand, at high velocities, the current can diffuse only a small distance, the resistance remains high, and the current is essentially confined to the corner.

The effect on temperature of lower current density is indicated in Fig. 14 where the isotherms for this case are shown. Note that the temperature is here considerably lower in the corner between sides S_1 and S_{10}, but is much the same as in Fig. 12 at other points in the armature.

Following page intentionally left blank

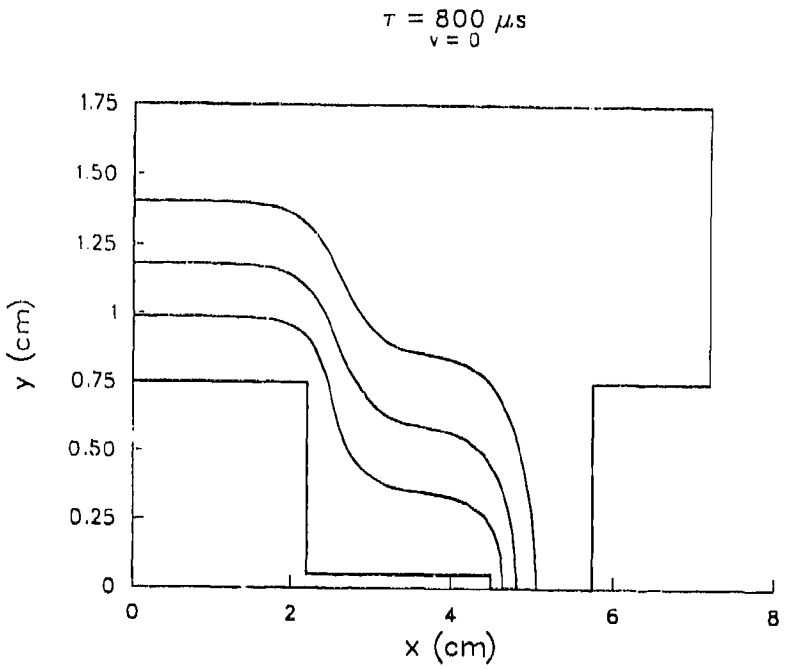

Figure 13. Current Streamlines at 800 μs for the Fixed Armature.

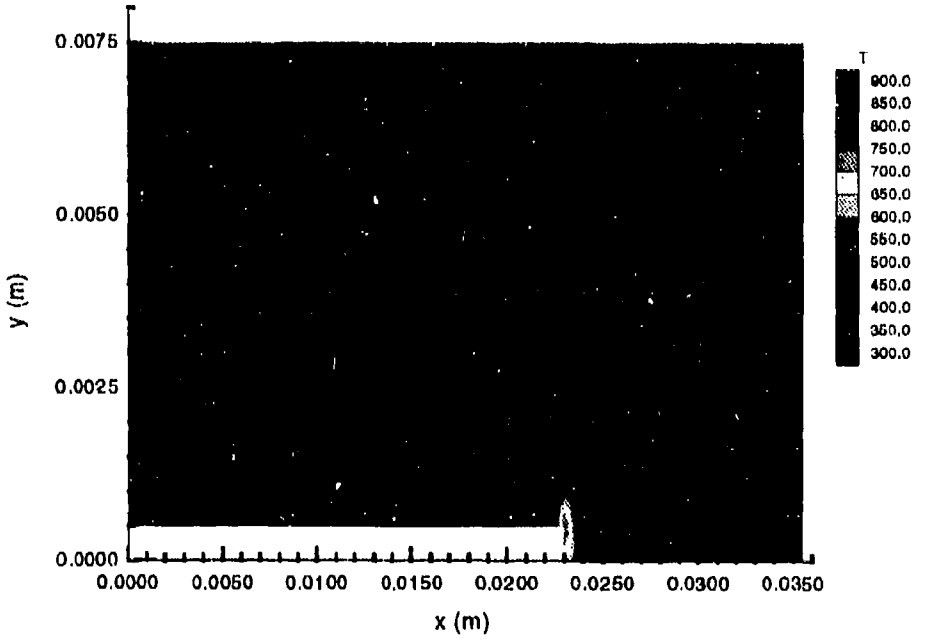

Figure 14. Isotherms at 800 μs for the Fixed Armature.

Following page intentionally left blank

4. SUMMARY, DISCUSSION, AND CONCLUSIONS

We have undertaken calculations to assess the effects of current and heat transport in the slotted armature as a function of time. As expected, the results indicated a large concentration of current near corners whose interior angle is greater than 180 degrees. The concentration is particularly high near the left-hand end of the interface between the rails and armature. The effects of this large-scale heating could presumably be ameliorated by rounding the troublesome corners, and we will attempt to undertake calculations for such armatures in future work. We have also undertaken some calculations for which the projectile was held fixed. The purpose of this work was to demonstrate the important effects that even small velocities can have on the results, and to demonstrate the ability of the model to predict the well-known velocity skin effect.

The most severe problems with the model at the present time seem to be the difficulty of performing calculations at high projectile velocities. The high velocities require an extremely small grid at the interface between the rails and the armature in order to resolve the high current concentration resulting from the velocity skin effect. In the explicit code, correspondingly smaller time steps are required to insure stability, and in the implicit version, more iterations are required to solve the difference equations at a given time. We do not believe, however, that there is any fundamental problem in using the model to solve these hypervelocity problems; the calculations just become time-consuming computationally.

As pointed out previously, there are also significant numerical problems near large-angle corners where the temperature and current-density gradients become very large. Unfortunately, these regions are the very places where we would like to have a reasonably accurate characterization of the temperature. In order to gain some insight into how significant the errors are we have undertaken the calculations here for a number different grids. In each case we have varied the grid spacing particularly close to those corners by a significant amount. We did, even for the smallest grids, observe rather significant changes in the corner temperature as the grid spacing varied. For the times for which the calculation was run, however, the changes incurred by varying the grid were largely confined to the corners themselves. It is possible that some better approximation could be undertaken in order to treat the corners more carefully. We have not investigated this possibility in detail since we regard the currents here to be more a physical problem rather than numerical one. In other words, sharp, large-angle corners are always going to produce unacceptably large temperatures and it is important to eliminate those corners in the design of projectiles.

A number of problems are slated for future study with this and similar models. First, we propose to extend the code to treat different types of geometry as well as to study aug-

mented railguns. Second, we intend to develop a better approximation for the temperature-dependent material properties and include, for example, the reduction in conductivity with melting. This smaller conductivity would permit more diffusion of the current into the rail at the corner of the armature-rail interface, and predict a less deleterious effect from the velocity skin effect. Third, it would be very advantageous to incorporate a model for the rail-armature interface that is more realistic than the perfect ohmic contact assumed here. Models for this interface which predict how current is transported across the surface have been discussed in the literature (Barber *et al.* 1991; James 1991). Finally, we propose to employ the output from these types of calculations in structural-analysis codes. The ultimate intention is to undertake for electromagnetic guns the same types of calculations that have been performed for more conventional guns.

5. REFERENCES

Ames, William F. *Numerical Methods for Partial Differential Equations.* New York:Academic, 1977, Chap. 5.

Barber, John P." The Acceleration of Macroparticles and a Hypervelocity Electromagnetic Accelerator," Ph. D. thesis, Australian National University, 1972 (unpublished).

Barber, John P. and A. Challita. "Velocity Effects on Metal Armature Contact Transition," *IEEE Trans. Magn.*, in press.

Barber, John P., A. Challita, B. Maas, and L. Thurmond. "Contact Transition in Metal Armatures." *IEEE Trans. Magn.*, Vol. MAG-27, pp. 228-231, 1991.

Hughes, W. F. and Young, F. J. "Transient and Steady-State Performance of the Laminated Armature for the Electromagnetic Launcher." Paper presented at the Air Force Armament Laboratory EM Gun Armature Workshop, Eglin AFB, FL, June 1986.

James, T. E. "Arcing Transition of Solid Armatures." *Third European Symposium on EML Technology*, p. 5-3-1, London, England, 1991.

Long, G. C. "Railgun Current Density Distributions." *IEEE Trans. Magn.*, Vol. MAG-22, pp. 1597-1602, November 1986.

Long, Glen C. "Fundamental Limits to the Velocity of Solid Armatures in Railguns." Doctoral Dissertation, University of Texas at Austin, Publication Number TD-35, August 1987.

Nearing, J. C. and M. A. Huerta. "Skin and Heating Effects of Railgun Current." *IEEE Trans. Magn.*, Vol. MAG-25, pp. 381-386, January 1989.

Putley, D. "Preliminary Investigations of the Velocity Skin Effect Using the PE2D Code, presented at the Seventh ELA Meeting, December 1989

Powell, John D. and Alexander E. Zielinski. "Theory and Experiment for an Ablating-Capillary Discharge and Application to Electrothermal-Chemical Guns." BRL-TR-3355, U. S. Army Ballistic Research Laboratory, Aberdeen Proving Ground, MD, June 1992.

Rodger, D. and P. J. Leonard. "Alternative Schemes for Electromagnetic Modelling of Rail Guns at Speed Using Finite Elements." *Proc. 3rd European Symposium on EML Technology*, London, England, 1991.

Rodger, D., P. J. Leonard, and J. F. Eastham. "Modeling Electromagnetic Rail Launchers at Speed Using 3D Finite Elements." *IEEE Trans. Magn.*, Vol. MAG-27, pp. 314-317, 1991.

Rodger, D., P. J. Leonard, J. F. Eastham, and S. P. Atkinson, "3D Finite Element Modeling of Electromagnetic Launchers." *Proc. 2nd European Symposium on EML Technology*, ISL St. Louis, France, 1989.

Young, F. J. and W. F. Hughes. "Rail and Armature Current Distributions in Electromagnetic Launchers."*IEEE Trans. Magn.*, Vol. MAG-18, pp.33-41, January 1982.

INTENTIONALLY LEFT BLANK.

No. of Copies	Organization
2	Administrator Defense Technical Info Center ATTN: DTIC-DDA Cameron Station Alexandria, VA 22304-6145
1	Commander U.S. Army Materiel Command ATTN: AMCAM 5001 Eisenhower Ave. Alexandria, VA 22333-0001
1	Director U.S. Army Research Laboratory ATTN: AMSRL-D 2800 Powder Mill Rd. Adelphi, MD 20783-1145
1	Director U.S. Army Research Laboratory ATTN: AMSRL-OP-CI-AD, Tech Publishing 2800 Powder Mill Rd. Adelphi, MD 20783-1145
2	Commander U.S. Army Armament Research, Development, and Engineering Center ATTN: SMCAR-IMI-I Picatinny Arsenal, NJ 07806-5000
2	Commander U.S. Army Armament Research, Development, and Engineering Center ATTN: SMCAR-TDC Picatinny Arsenal, NJ 07806-5000
1	Director Benet Weapons Laboratory U.S. Army Armament Research, Development, and Engineering Center ATTN: SMCAR-CCB-TL Watervliet, NY 12189-4050
(Unclass. only) 1	Commander U.S. Army Rock Island Arsenal ATTN: SMCRI-IMC-RT/Technical Library Rock Island, IL 61299-5000
1	Director U.S. Army Aviation Research and Technology Activity ATTN: SAVRT-R (Library) M/S 219-3 Ames Research Center Moffett Field, CA 94035-1000

No. of Copies	Organization
1	Commander U.S. Army Missile Command ATTN: AMSMI-RD-CS-R (DOC) Redstone Arsenal, AL 35898-5010
1	Commander U.S. Army Tank-Automotive Command ATTN: ASQNC-TAC-DIT (Technical Information Center) Warren, MI 48397-5000
1	Director U.S. Army TRADOC Analysis Command ATTN: ATRC-WSR White Sands Missile Range, NM 88002-5502
1	Commandant U.S. Army Field Artillery School ATTN: ATSF-CSI Ft. Sill, OK 73503-5000
(Class. only) 1	Commandant U.S. Army Infantry School ATTN: ATSH-CD (Security Mgr.) Fort Benning, GA 31905-5660
(Unclass. only) 1	Commandant U.S. Army Infantry School ATTN: ATSH-CD-CSO-OR Fort Benning, GA 31905-5660
1	WL/MNOI Eglin AFB, FL 32542-5000
	Aberdeen Proving Ground
2	Dir, USAMSAA ATTN: AMXSY-D AMXSY-MP, H. Cohen
1	Cdr, USATECOM ATTN: AMSTE-TC
1	Dir, ERDEC ATTN: SCBRD-RT
1	Cdr, CBDA ATTN: AMSCB-CI
1	Dir, USARL ATTN: AMSRL-SL-I
10	Dir, USARL ATTN: AMSRL-OP-CI-B (Tech Lib)

No. of Copies	Organization
4	Commander U.S. Army Armament Research, Development, and Engineering Center ATTN: SMCAR-FSE, Bldg. 329 Riccardo Brognara Mr. William H. Davis SMCAR-FSA-E, Dr. T. Gora John Bennett Picatinny Arsenal, NJ 07806-5000
4	Commander U.S. Army Armament Research, Development, and Engineering Center ATTN: SMCAR-CCL-FA, H. Moore H. Kahn W. Williams B. Schlenner Bldg. 65N Picatinny Arsenal, NJ 07806-5000
1	Director Benet Laboratories ATTN: SMCAR-CCB-RT, Peter D. Aalto SMCAR-CCB-RM, Dr. Pat Vottis Watervliet, NY 12189
1	Director DARPA ATTN: Dr. Peter Kemmey 3701 North Fairfax Drive Arlington, VA 22203-1714
1	Commander SDIO ATTN: SDIO/IST, MAJ M. Huebschman Washington, DC 20301-7100
3	CG, MCRDAC Code AWT ATTN: Dr. C. Vaughn Mr. G. Solhand MAJ F. Wysocki Quantico, VA 22134-5080

No. of Copies	Organization
1	Director U.S. Army Research Office ATTN: Dr. Michael Ciftan P.O. Box 12211 Research Triangle Park, NC 27709-2211
1	WL/MNSH ATTN: Donald M. Littrell James Brion Cornette Site A-15 Eglin AFB, FL 32542-5434
1	Director Brookhaven National Laboratory ATTN: Dr. J. R. Powell Bldg. 129 Upton, NY 11973
1	Director Lawrence Livermore National Laboratory ATTN: Dr. R. S. Hawke, L-156 P.O. Box 808 Livermore, CA 94550
2	Director Los Alamos National Laboratory ATTN: MSG 787, Dr. J. V. Parker Los Alamos, NM 87545
1	Director Sandia National Laboratories ATTN: Dr. Maynard Cowan Dept. 1220 P.O. Box 5800 Albuquerque, NM 87185
2	Maxwell Laboratories ATTN: Dr. Rolf Dethlefson Dr. Ian McNab 8888 Balboa Ave. San Diego, CA 92123
1	GA Technologies, Inc. ATTN: Dr. L. Holland P.O. Box 85608 San Diego, CA 92138

No. of Copies	Organization
1	Electromagnetic Research, Inc. ATTN: Dr. Peter Mongeau 2 Fox Road Hudson, MA 01749
2	IAP Research, Inc. ATTN: Dr. John P. Barber Mr. David P. Bauer 2763 Culver Ave. Dayton, OH 45429-3723
2	LTV Aerospace & Defense Company ATTN: MS TH-83, Dr. Michael M. Tower Dr. G. Jackson P.O. Box 650003 Dallas, TX 75265-0003
1	Science Applications International Corporation ATTN: Dr. K. A. Jamison 1247-B North Eglin Parkway Shalimar, FL 32579
1	FMC Corporation Mailstop M170 ATTN: Brad Goodell 4900 East River Road Minneapolis, MN 55421-1498
3	Science Applications International Corporation ATTN: Dr. Jad H. Batteh Dr. G. Rolader Mr. L. Thornhill 1503 Johnson Ferry Rd., Suite 100 Marietta, GA 30062
1	Westinghouse Science and Technology Center ATTN: Mr. Doug Fikse 1310 Beulah Road Pittsburgh, PA 15233
1	Auburn University Leach Nuclear Science Center Department of Physics ATTN: Dr. Raymond F. Askew Auburn University, AL 36849-5301

No. of Copies	Organization
1	Auburn University ATTN: Dr. Eugene Clothiaux 206 Allison Lab Auburn University, AL 36849-5311
1	Texas Technical University Department of EE/Computer Science ATTN: Dr. M. Kristiansen Lubbock, TX 79409-4439
1	Texas Technical University Department of Elect Eng M/S 3102 ATTN: Dr. Mary Baker Lubbock, TX 79409-4439
3	Institute for Advanced Technology The University of Texas at Austin ATTN: Dr. M. D. Driga Dr. Harry Fair Dr. Kuo-Ta Hsieh 4030-2 W. Braker Lane Austin, TX 78759-5329
1	University of Miami Department of Physics ATTN: Dr. Manuel A. Huerta P.O. Box 248046 Coral Gables, FL 33124
1	North Carolina State University Department of Nuclear Engineering ATTN: Dr. John Gilligan P.O. Box 7909 Raleigh, NC 27695
1	Center for Laser App. Eng. Sci & Mechanics University of Tennessee Space Institute, Mail Stop 14 ATTN: Dr. Dennis Keefer B. H. Goethert Parkway Tullahoma, TN 37388-8897
2	Center for Electromechanics University of Texas at Austin ATTN: Mr. Siddharth B. Pratap Mr. John H. Price 10100 Burnet Road, Bldg. 133 Austin, TX 78748

No. of Copies	Organization
1	Supercon Inc. ATTN: Charles Renaud 830 Boston Turnpike Road Shrewsbury, MA 01545
	Aberdeen Proving Ground
1	Cdr, USATECOM ATTN: AMSTE-SI-F

USER EVALUATION SHEET/CHANGE OF ADDRESS

This Laboratory undertakes a continuing effort to improve the quality of the reports it publishes. Your comments/answers to the items/questions below will aid us in our efforts.

1. ARL Report Number ARL-TR-74 Date of Report February 1993

2. Date Report Received _____

3. Does this report satisfy a need? (Comment on purpose, related project, or other area of interest for which the report will be used.) _____

4. Specifically, how is the report being used? (Information source, design data, procedure, source of ideas, etc.) _____

5. Has the information in this report led to any quantitative savings as far as man-hours or dollars saved, operating costs avoided, or efficiencies achieved, etc? If so, please elaborate. _____

6. General Comments. What do you think should be changed to improve future reports? (Indicate changes to organization, technical content, format, etc.) _____

CURRENT ADDRESS

_____
Organization

_____
Name

_____
Street or P.O. Box No.

_____
City, State, Zip Code

7. If indicating a Change of Address or Address Correction, please provide the Current or Correct address above and the Old or Incorrect address below.

OLD ADDRESS

_____
Organization

_____
Name

_____
Street or P.O. Box No.

_____
City, State, Zip Code

(Remove this sheet, fold as indicated, staple or tape closed, and mail.)

DEPARTMENT OF THE ARMY

OFFICIAL BUSINESS

BUSINESS REPLY MAIL
FIRST CLASS PERMIT No 0001, APG, MD

Postage will be paid by addressee

Director
U.S. Army Research Laboratory
ATTN: AMSRL-OP-CI-B (Tech Lib)
Aberdeen Proving Ground, MD 21005-5066

NO POSTAGE
NECESSARY
IF MAILED
IN THE
UNITED STATES